Effect of the Neutron and Heavy-ion Irradiation on the Pinning Properties of Cuprate Superconductors

Noriko Chikumoto

1 Introduction

Critical current density (J_c), the maximum current density we can pass with zero resistance, is one of the most important properties for application of superconductors. Because the resistivity in superconductor is caused by vortex motion due to the Lorentz force from passed electric current, it is necessary to introduce so-called pinning centers that prevent the vortex motion. So a lot of efforts have been made to explore pinning centers that provide strong pinning force (F_p) to improve J_c. It is widely known that imperfections in superconducting matrix, such as normal precipitates, grain boundaries, dislocations, stacking faults, etc., can be pinning centers. At such imperfections, the depression of superconducting order parameter occurs. When the vortex passes through the imperfections, the energy of vortices changes, resulting in a vortex pinning interaction.

Irradiation of a material with particles, such as electrons, protons, neutrons, and ions, has known to be a useful way to introduce defects in a controlled way; the sizes and the densities of the irradiation defects can be changed by irradiation conditions such as kind, energy, and fluence of radiated particles. The greatest advantage of this method is that it can be used independently of the material synthesis process.

Among various kinds of irradiation, the high-energy heavy-ion irradiation is attracted much attention, since it produces columnar defects that is expected to give strongest pinning force if the flux line is aligned with their length direction. On the other hand, the neutron irradiation has an advantage of a large penetration range. It

N. Chikumoto (✉)
Center of Applied Superconductivity and Sustainable Energy Research, Chubu University, Kasugai, Japan
e-mail: nchiku@isc.chubu.ac.jp

A. G. Roca et al. (eds.), *Surfaces and Interfaces of Metal Oxide Thin Films, Multilayers, Nanoparticles and Nano-composites*,
https://doi.org/10.1007/978-3-030-74073-3_8

is also expected to introduce effective pinning centers, because the size of neutron damage is comparable to the size of the vortex core.

A great deal of irradiation experiment has been performed since the discovery of the high T_c superconductors and there are a plenty of reports on it [1]. So in this chapter, I would like to show some data that are not much studied. This chapter is organized as follows. First the basic understandings regarding the introduction of defects by irradiation will be explained. Then we show some of our experimental result of neutron and the heavy-ion irradiation effects on the pinning properties of two kinds of cuprate high T_c superconductors (HTSC), $(La_{1-x}Sr_x)_2CuO_{4-\delta}$ (La214) and $REBa_2Cu_3O_{7-\delta}$ (RE123, RE:Y, Nd, Gd). In La214, the neutron and heavy-ion irradiation effect on the J_c-B characteristics was investigated using single crystal samples. On the other hand, in RE123, we performed irradiation studies using coated conductors. We only performed heavy-ion irradiation, but the irradiation conditions, irradiation species, etc., were changed in order to change the size, length, and the arrangement of irradiation defects. In addition, we performed oxygen annealing to examine the stability of irradiation defects.

2 Defects Introduced by Irradiation

The effects of radiation on crystalline solids are highly variable depending on the type of material and the type of incident radiation. However, there are roughly two effects. One is the ionization and electronic excitation often results in chemical reactions and finally disappears. The other is the knocking-on the atom to cause the atomic displacement. This effect is very important because it results in the radiation damages that remain in the crystal and often causes the change of the material properties. These two effects are derived from nuclear energy loss and electric energy loss of radiation in condensed matter, and the contribution of each phenomenon differs among the kind and the energies of the incident particles. In the case of electron and proton irradiation, electric energy loss is dominant. They may produce point-like defects in the form of interstitial ions and vacancies (Frenkel pairs). On the other hands, nuclear energy loss is also important in the case of ions and neutrons and larger defects are created, as follows.

Neutron irradiation is generally carried out by exposing a material in a fission reactor that provides a wide spectrum of neutrons. Defect cascades are mainly produced by fast neutrons with energies above 0.1 MeV. According to the transmission electron microscope (TEM) observation reported in Ref. [2], the major observable defects introduced by the neutron irradiation are spherical collision cascades, with sizes ranging from below 1 nm up to 5 nm in diameter, surrounded by the strain field. Since the size of cascade defects is comparable to the coherence length of HTSC's, it yields a preferable condition for core pinning. Indeed, large improvements of pinning properties had been reported for various HTSC by several groups [3]. On the other hand, the lower energy neutrons may create small size defects,

such as point defects (Frenkel pairs) and defect clusters. It mainly results in the oxygen disordering and causes the depression of T_c [4].

In case of high-energy ion irradiation, the incident ions give energy to the target material through the electric energy loss procedure and slow down themselves. So the extent of the electronic energy loss is often called to be the electron stopping power, S_e. It is known that the damage morphology strongly depends on the electronic stopping power S_e of the incident in the target. For instance, in the case of Y123 polycrystalline samples, discontinuous extended defects are introduced when the S_e exceeds the threshold value of » 8 keV/nm [5]. As S_e increases, the defects are more elongated and finally the continuous columnar defects are created at $S_e >$ 20 keV/nm [5].

Figure 1 shows typical columnar defects in Nd123 single crystal observed by TEM. The irradiation was carried out at Grand Accélérateur National d'Ions Lourds (GANIL) (Caen, France) using 5.8 GeV Pb-ion. Direction of the incident beam was parallel to the crystal *c*-axis. Figure 1a is the plan-view of the columnar defects. The defects are seen as white contrasts. The amorphous regions with diameter » 7 nm are randomly distributed in the sample. The incident ion beam crossed the whole thickness of the sample < 100 μm and create parallel continuous columnar defects (Fig. 1b).

It is noteworthy that such irradiation defects are also influenced strongly by the irradiation temperature. At very low temperature, the defects cannot move, but above a particular temperature, rearrangement or recombination of defects occurs through thermal diffusion process. It causes the formation of some kinds of complex defect clusters such as dislocation loops and stacking faults instead of annihilation.

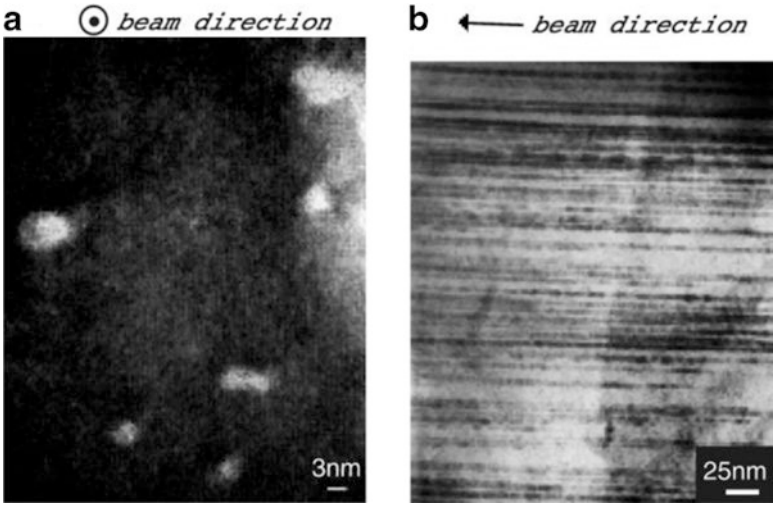

Fig. 1 Transmission electron micrographs of columnar defects in the 5.8 GeV Pb-ion irradiated Nd123 single crystal. (**a**) TEM image of the track cross-section. (**b**) Images taken along the columnar defects

Radiochemical effects during irradiation make the situation more complicated. Local heating effects by thermal spikes, etc., are expected to accelerate the moving of interstitial atoms and vacancies. Important point is that the radiation damages might be modified or even recovered by annealing the irradiated material at a certain temperature.

3 Irradiation Effects in La214 Single Crystals

3.1 Neutron Irradiation of La214 Single Crystal

In HTSC, it has been recognized that the electronic anisotropy and the interlayer coupling between superconducting CuO_2 layers affect their magnetization behaviors in the mixed state. Among various kinds of HTSC, $(La_{1-x}Sr_x)_2CuO_{4-\delta}$ (La214) is known to have the simplest crystal structure with only one CuO_2 plane. In this system, the anisotropy can be varied by changing the Sr content, x. According to resistivity measurement reported by Kimura et al. [6], the anisotropy ratio ρ_c/ρ_{ab} at 50 K decreased drastically from nearly 4000 to 160 with increasing x. Kobayashi et al. [7] reported that the magnetization behavior of the crystal also changes with x. In the under-doped crystal, $x < 0.075$, hysteresis width, ΔM, decreases exponentially with the applied magnetic field. On the other hand, in the over-doped crystal, $x > 0.075$, an anomaly in magnetization curves, in particular the depression of the magnetization at intermediate field range followed by a secondary maximum ("the second peak effect") is observed, when the magnetic field was applied perpendicular to the CuO_2 plane.

Similar second peak effect has been reported in various high T_c superconductors (HTSC), such as RE123 [8–10], $YBa_2Cu_4O_{8-\delta}$ (Y124) [11], Bi2212 [12–15], and Tl-based compounds [16]. Several mechanisms have been proposed to explain "the second peak effect": (1) second phase such as oxygen-deficient region is driven normal by applied field and start to act as additional pinning centers [8]. (2) A change in flux creep dynamics [9, 12]. (3) 3D-2D transition in the vortex system [15] (4) Matching of vortex spacing to pinning center periodicity ("matching effect") [14], (5) the field-driven disordering transition from Bragg glass phase to vortex glass phase [10].

Considering the facts that the secondary peak is observed only for over-doped compositions in La214 and a substantial amount of the oxygen deficiency is reported to exist only in the over-doped composition of La214 [17]; this behavior is likely to be attributed to the existence of oxygen defects. So we investigated the effect of neutron irradiation on the secondary peak in the over-doped La214 crystals, in an attempt to reveal the role of defects in this phenomenon.

In this study, we used the La214 single crystal with $x = 0.11$ grown by a travelling-solvent floating-zone (TSFZ) method. The details of crystal growth are described in details in Ref. [6]. The sample was sequentially irradiated with neutrons to the

fluences of 2 and 4×10^{20} m^{-2}. The irradiations were carried out in a nuclear research reactor (JRR-4) at Japan Atomic Energy Research Institute. The flux density of fast neutron was about 5.5×10^{16} m^{-2}s^{-1}. During the irradiation, the sample was wrapped with quartz wool and enclosed in an evacuated quartz tube. The number of the displacement of the atoms due to the irradiation is calculated to be less than 10^{-4} d.p.a. (displacement per atom) at the fluence of 4×10^{20} m^{-2}, and there was no observable change in T_c (~ 29.4 K) after each irradiation. Magnetization measurements were performed by a Vibrating Sample Magnetometer (VSM, EG&G Princeton Applied Research, Model 4500), with applied magnetic fields parallel to the c-axis. The field sweep rate during the magnetization measurement had been kept at 20 mT/s.

Typical magnetization curves recorded at $T = 15$ K for La214 single crystal with $x = 0.11$ before and after the neutron irradiations are shown in Fig. 2. The height of the secondary peak was strongly enhanced and the secondary peak field, B_{pk}, was shifted downward, after the neutron irradiation. On the other hand, there was no observable change in the hysteresis width for $B_a > B_{pk}$.

The temperature dependence of the magnetization curves of the irradiated sample with the fluence of 2×10^{20} m^{-2} is shown in Fig. 3. The secondary peak appears over a wide temperature range from 4.2 K to near T_c. The peak position shifts to lower fields as the temperature is increased, similar to that observed in the unirradiated sample [7]. Similar behavior was also observed in the irradiated sample with the fluence of 4×10^{20} m^{-2}.

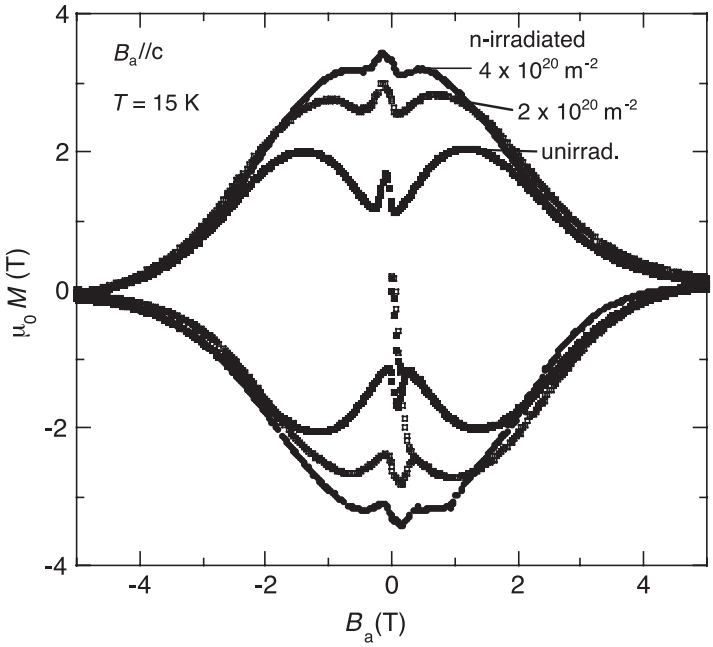

Fig. 2 Magnetization curve of $(La_{0.89}Sr_{0.11})_2CuO_{4-\delta}$ recorded at T=15 K before and after neutron irradiation. The neutron fluences were 2 and 4×10^{20} m^{-2}

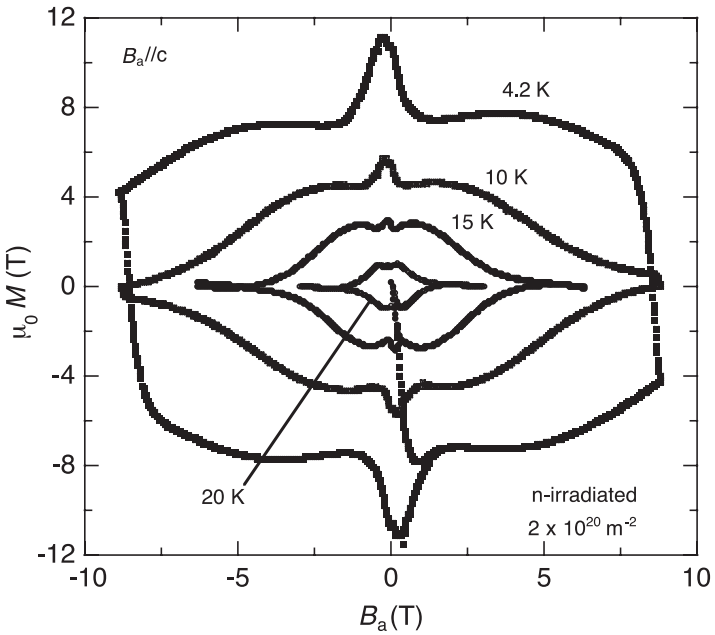

Fig. 3 Temperature dependence of magnetization curves for neutron-irradiated La214 ($x = 0.11$) crystal (fluence: 2×10^{20} m^{-2})

Figure 4 shows the temperature variation of the observed B_{pk} and the irreversibility field, B_{irr}, where B_{irr} was determined from the locus of the vanishing of hysteresis width. The downward shift of B_{pk} by the irradiation was observed over a wide temperature range. On the other hand, B_{irr} was unchanged after each irradiation step. This result indicates that introduced defect cascades play an important role in the low and the intermediate field range where we observe the secondary peak, but it is not effective for raising B_{irr}.

Kobayashi et al. found that the temperature dependence of B_{pk} can be expressed by,

$$B_{pk}^{1/2} = A\left(T - T_c\right) \tag{1}$$

where T_c is critical temperature, A is an arbitrary constant [7]. So the square root of B_{pk} is plotted as a function of temperature in Fig. 5, in order to see the applicability of (1) in the irradiated samples. It can be seen that the square root of B_{pk} of irradiated samples also exhibit a linear relation with the temperature. This result indicates that the secondary peaks observed in the irradiated samples are due to the same mechanism as that in the unirradiated sample.

Further insight into the efficiency of defect cascades introduced by the neutron irradiation is given by analyzing the pinning force density, F_p, by the irradiation. Figure 6 shows the magnetic field variation of F_p at $T = 15$ K calculated from the data shown in Fig. 3. While F_p increases at low fields with increasing the irradiation

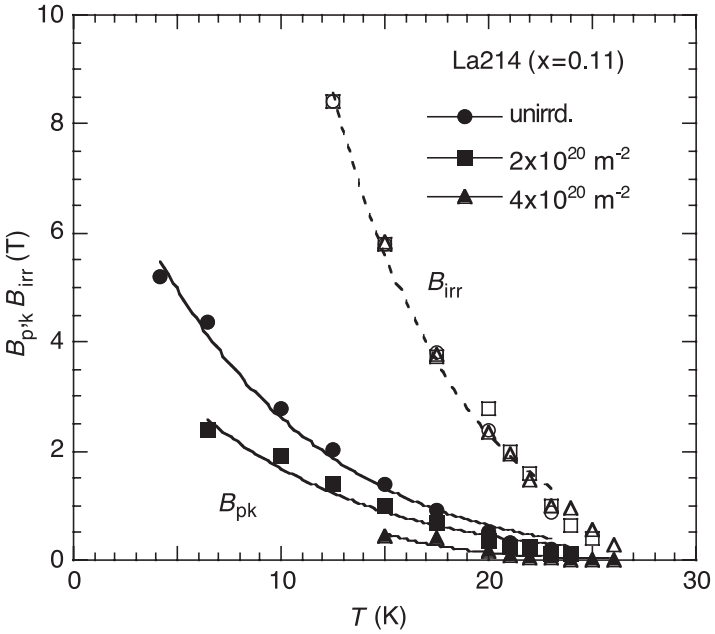

Fig. 4 The temperature variation of B_{pk} and B_{irr} of unirradiated and neutron-irradiated La214 crystal (x=0.11)

fluence, it saturated at high fields. At high fields, F_p decreases as $1 - B/B_{irr}$ with the increasing field. Such a saturation behavior has been often observed in the conventional superconductors with rather weak pinning centers [18]. Matsushita et al. [19] explained such a behavior in terms of avalanching depinning model. The flux lattice is considered to contain many defects, and local plastic deformations may take place under the driving force. If the pinning is not strong enough, such a local instability might develop to a catastrophic avalanching flux flow. The probability of occurrence of a plastic deformation is considered to be proportional to defects of flux lattice. As for the intermediate field region, just below the peak field, deformation of the flux lattice allows the vortices to be pinned most effectively ("synchronization effect") and increase in pinning strength is expected. This may be the possible origin of the secondary peak phenomenon. However, further discussion is needed.

3.2 Heavy-Ion Irradiation of La214 Single Crystals

For heavy-ion irradiation experiment, we used two La214 single crystals with different Sr contents, x = 0.05 (under-doped) and 0.11 (over-doped). Both of them were grown by a travelling-solvent floating-zone (TSFZ) method [5]. The irradiation with 5.8 GeV Pb-ions was performed at GANIL at room temperature. Direction

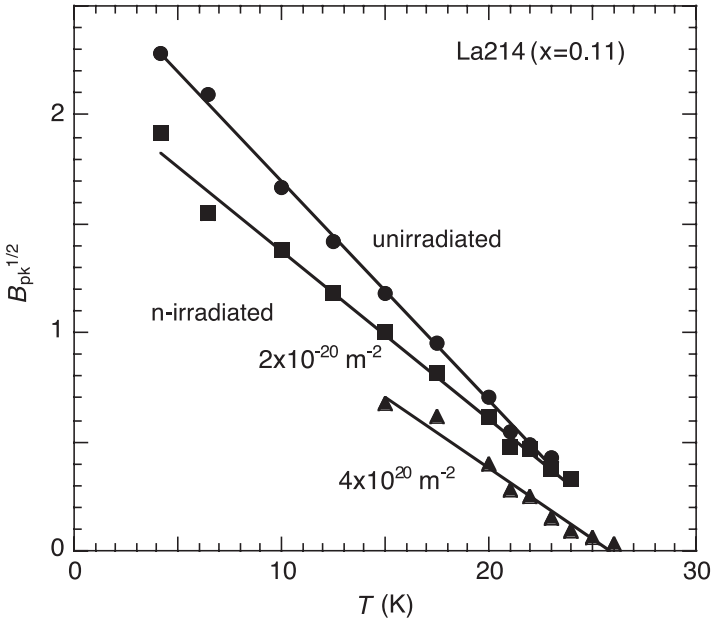

Fig. 5 Temperature dependence of the square root of B_{pk}

of the incident beam was almost parallel to the c-axis. The samples were sequentially irradiated to the fluences of 10^{10} and 1.1×10^{11} ions/cm^2, corresponding to a dose-equivalent flux density of $B_\Phi = 0.2$ and 2.2 T, respectively.

Firstly, we show the irradiation effect in under-doped La214. Figure 7 shows typical magnetization curves of Pb-ion irradiated La214 crystals ($x = 0.05$) measured at $T = 10$ K. Total irradiation fluences were $B_\Phi = 0.2$ and 2.2 T. In the $B_\Phi = 0.2$ T sample, a double-peak structure appeared at low field and it shifted toward higher field after the higher dose irradiation ($B_\Phi = 2.2$ T). Owing to this peak structure, the lightly irradiated sample showed a larger hysteresis at low fields.

The temperature dependence of the magnetization curves of the irradiated samples ($B_\Phi = 0.2$ and 2.2 T) is shown in Fig. 8. In the $B_\Phi = 0.2$ T sample, the double-peak structure appears at temperature above 10 K, while the $B_\Phi = 2$ T sample exhibits double-peak structure at whole temperature range from 4.2 K to T_c. It was found that the peak field is almost independent of temperature.

Next, we show the irradiation effect in over-doped La214. Figure 9 presents typical magnetization curves of unirradiated and Pb-ion irradiated La214 sample ($x = 0.11$), recorded at 10 K. Total fluences were $B_\Phi = 0.2$ and 2.2 T. After the irradiation, the hysteresis width is dramatically enhanced at low field range, while only a slight change was observed in the high fields.

In the magnetization curves of the heavily Pb-ion irradiated crystal ($B_\Phi = 2.2$ T), a new peak structure appeared at lower field. This new peak is very sharp and its position was found to be temperature independent, similar to that observed in the

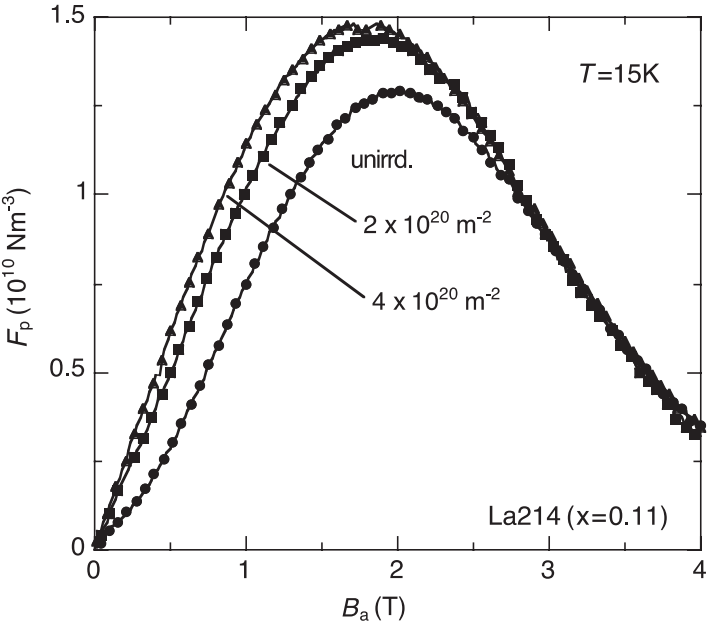

Fig. 6 Magnetic field variation of pinning force density, F_p, at $T = 15$ K before and after the neutron irradiation

irradiated La214 crystals with under-doped composition ($x = 0.05$). Moreover, the peak field was same as that of under-doped sample with the same irradiation dose ($B_\Phi = 2.2$ T). As far as the temperature dependence is concerned, the origin of this new peak is different from that of the secondary peak, which exhibits strong temperature dependence, as shown previously.

Figure 10 compares the effect of the irradiation on the irreversibility field, B_{irr} for $x = 0.05$ and 0.11 samples. The irreversibility field was determined from the closing point of hysteresis loop. In $x = 0.05$ sample, a slight increase of B_{irr} with irradiation fluence was observed at an intermediate temperature range. Decrease of B_{irr} above 20 K observed in $B_\Phi = 2.2$ T sample is due to the degradation of T_c, from 27.5 K to 24.8 K. On the other hand, irreversibility line was almost unchanged in case of $x = 0.11$ sample. The difference in irradiation effect on B_{irr} between the two samples can be explained by the difference of pre-existing defects. In $x = 0.05$, pinning strength of the pre-existing defects is very weak and B_{irr} is much lower than $x = 0.11$. In this case, introduction of strong pinning center by irradiation effectively increases. On the other hand, in $x = 0.11$ the effect of introducing irradiation defects hardly appeared, since there were already sufficiently strong pinning centers.

Now we discuss the origin of the peak in magnetization curves observed in heavy-ion irradiated La214 samples. The peak observed in the Pb-ion irradiated sample exhibits four distinct features:

1. The peak has a very sharp structure,

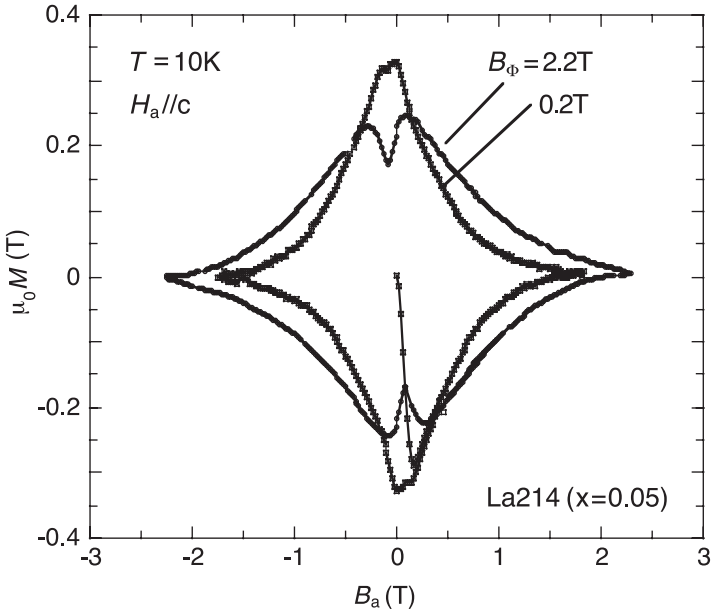

Fig. 7 Magnetization curves of Pb-ion irradiated La214 crystals (x = 0.05) (B_Φ = 0.2, 2.2 T) recorded at T =10 K

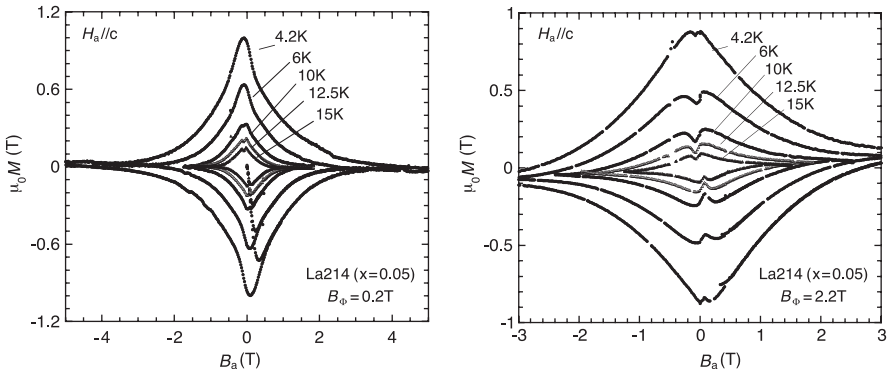

Fig. 8 Temperature dependence of magnetization curves of Pb-ion irradiated under-doped La214 crystals (x = 0.05) (B_Φ = 0.2, 2.2 T)

2. The peak field is independent of temperature,
3. The samples with the same irradiation fluence have the same peak field, independent of sample composition,
4. The peak moves to higher fields with increasing irradiation fluence.

The peak was also appeared in the unirradiated sample with the over-doped composition. However, it showed completely different characteristics: The peak appears

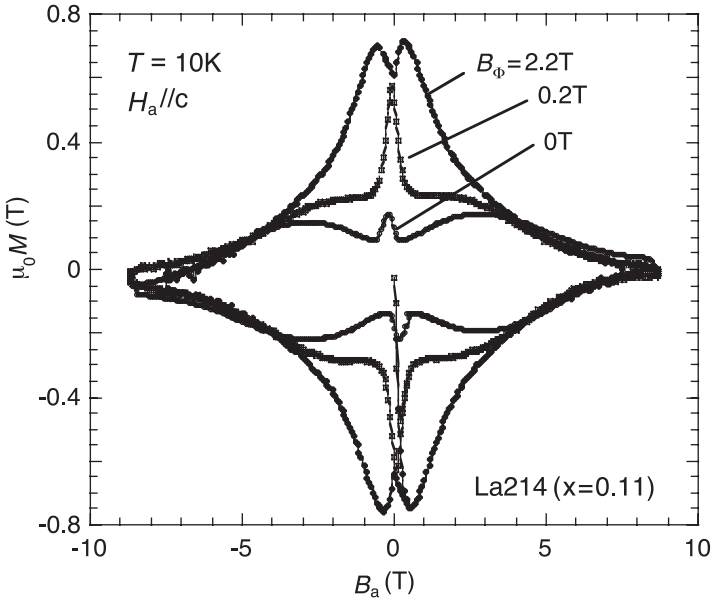

Fig. 9 Magnetization curves of unirradiated and Pb-ion irradiated (B_Φ = 0.2, 2.2 T) La214 crystals (x = 0.11) recorded at T =10 K

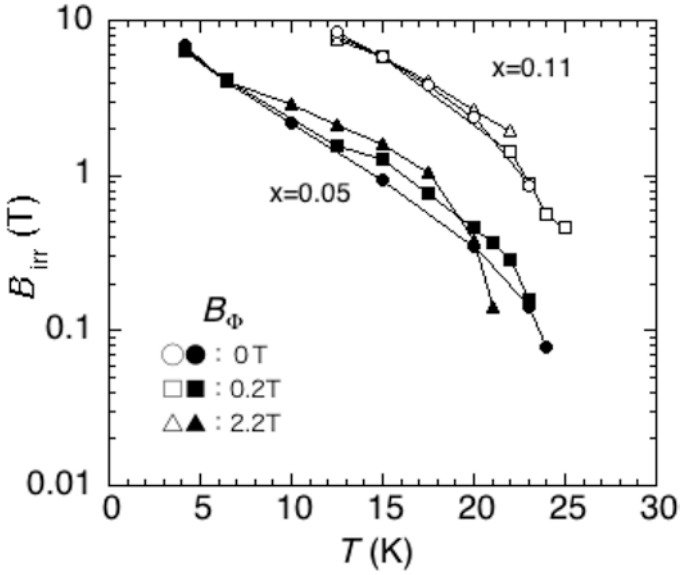

Fig. 10 The irreversibility line of unirradiated and Pb-ion irradiated La214 crystals (x=0.05 (closed symbols) and 0.11(open symbols))

at an intermediate field which is strongly temperature dependent. And it has rather broad structure. Therefore, we suppose that the peak appeared in the Pb-ion irradiated sample has a different origin from that in the unirradiated sample. Several mechanisms have been proposed to explain peak effect as shown previously. Among them, the present observation seems to be consistent with the matching effect mechanism. Since a matching of flux lattice to a periodic distribution of pinning center is expected to occur at constant value of the magnetic field, the peak position should not show any temperature dependence. The shift of peak field after the higher dose irradiation is also consistent with such a picture.

In the case of heavy-ion irradiated samples, pinning of flux lattice is mainly due to randomly distributed columnar defects. Even if the array of pinning center is not perfectly periodic, matching effect is expected to occur when the mean vortex spacing matches the mean spacing of pinning center, in the case of rather concentrated system of pinning centers. It is reasonable then that such matching peak appears at lower field than calculated value of B_Φ.

4 Irradiation Effects in RE123 Coated Conductors

4.1 Effect of Heavy-Ion Irradiation in RE123 Coated Conductors

Since RE123 coated conductors have relatively excellent high magnetic field characteristics among various HTSCs, it is expected to be applied to magnets. So a number of studies have been conducted to explore a new method to introduce effective pinning centers that can improve J_c at high magnetic field. Most of the introduction methods are based on chemical methods. The most common way is adding impurities to a raw material and dispersing it as a precipitate in superconducting RE123 phase during the manufacturing process. In the pulsed laser deposition method (PLD method), it has been reported that the $BaMO_3$ (M=Hf, Zr, Sn) inclusion form long columnar inclusion with its diameter ~10 nm within RE123 matrix and they provide considerable J_c enhancement at high magnetic fields [20–22]. For the further enhancement of J_c, we need to optimize many parameters, such as size, shape, arrangement, inclement, density of pinning centers. However, it is difficult to control these parameters in case of chemical method.

On the other hand, the irradiation method has the advantage that these parameters can be controlled independently of the manufacturing process of the coated conductors. In this method, the damage morphology strongly depends on the electronic stopping power, S_e. In the case of Y123 polycrystalline samples, the continuous columnar defects are created at $S_e > 20$ keV/nm [5]. It has also been reported that the diameter of columnar defect increases with S_e [23]. Since the size and shape of columnar defects are very similar to $BaMO_3$ nano-rods, this technique can be used to create a model system for pinning optimization.

Therefore, in this study, we used the heavy-ion irradiation technique to explore an optimum condition for improving J_c in RE123 tape.

In the present study, we used Y123 tape prepared by a pulsed laser deposition (PLD) technique. The dimension of each layer of the tape used in the present study is as follows: Ag (5 μm), Y123 (0.5 μm), CeO_2 (0.55 μm), $Gd_2Zr_2O_7$ (0.8 μm), and Hastelloy (100 μm). One-cm-width tape was cut into the size of about 2.0 mm × 2.0 mm, and they were irradiated either by 450 MeV $^{129}Xe^{23+}$, 500 MeV $^{197}Au^{31+}$, or 400 MeV $^{84}Kr^{18+}$ ions to the Y123 layer from Ag layer side by using the AVF cyclotron of Japan Atomic Energy Agency. In order to change the energy of heavy ions incident to the Y123 layer, Ag layer of some sample was removed by a chemical etching method. The irradiation fluence was varied from 1.0×10^{10} to 1.0×10^{12} ions/cm^2, while the direction of the incident beam was kept for perpendicular to the tape surface (parallel to the *c*-axis of Y123 layer.

We also calculated S_e in Y123 layer by using TRIM code (TRansport of Ion in Matter). For calculations, we assumed that the composition of the Y123 layer is $YBa_2Cu_3O_{6.9}$, density is 6.5 g/cm^3 and the displacement energy E_d = 20 eV [24]. Calculated results are shown in Fig. 11. We can say from the calculation that introduced ions have enough energy to penetrate Y123 layer, and S_e is almost constant within the Y123 layer in each condition.

We also estimated the diameter of columnar defects from Ref. 21. Irradiation conditions and corresponding S_e values and estimated diameter of columnar defects are summarized in Table 1.

Before and after the irradiation, magnetic hysteresis measurement was performed with physical property measuring system (PPMS), Quantum design, and J_c was

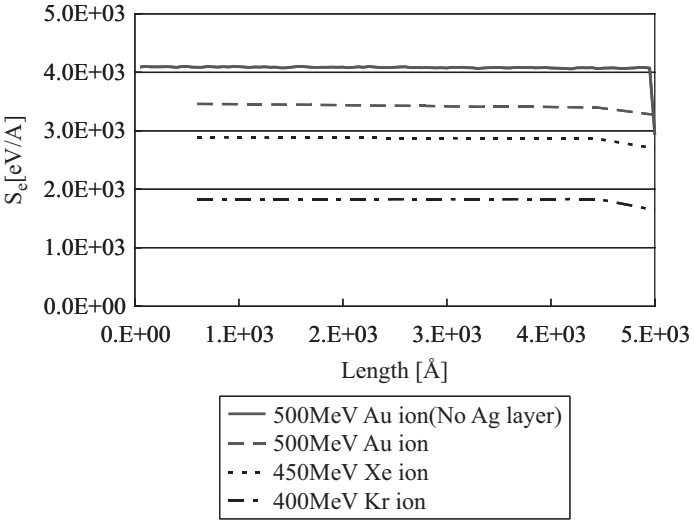

Fig. 11 S_e in Y123 layer for 500 MeV Au-ion, 450 MeV Xe-ion, and 400 MeV Kr ion irradiation. The calculation was carried out using TRIM code (TRansport of Ion in Matter), assuming Y123 is covered by 5 μm of Ag layer

Table 1 Irradiation conditions, calculated S_e values and diameter of columnar defects

	Thickness of Ag on top of Y123 (μm)	S_e (keV/nm)	Estimated diameter of columnar defects (nm)
400 MeV $^{84}Kr^{18+}$	5.0	18	4
450 MeV $^{129}Xe^{23+}$	5.0	29	8
500 MeV $^{197}Au^{31+}$	0	41	13
	5.0	34	11

calculated using modified Bean model [25]. T_c was determined from AC susceptibility measurement.

At first, we show typical columnar defects observed by TEM for Xe-ion and Au-ion irradiated Y123 tapes in Fig. 12. In both cases, the continuous columnar defects (shown by arrows) are successively created in the Y123 layer.

Figure 13 shows the fluence dependence of J_c at $T = 77$ K and for applied magnetic field $B_a = 0.2$ and 2 T for Kr, Xe and Au-ion irradiation. At $B_a = 0.2$ T, J_c was most improved at 1×10^{11} ions/cm^2 in all irradiations except Kr, and the degree of increase was almost constant regardless of the ion species. On the other hand, at $B_a = 2$ T, the largest improvement in J_c was observed in the higher fluence region (3 to 5×10^{11} ions/cm^2), and the maximum value of J_c varies with ion species. We can also see that the Xe-irradiation is most effective for enhancement of high field J_c. It is noteworthy that the defect diameter of Xe-irradiation is not largest among three species.

Here, we would like to define the fluence at which the maximum improvement in J_c is obtained at each applied magnetic field B_a as "optimum fluence (ϕ_{op} (B_a))." Then we consider the relationship between the density of the columnar defects and the applied magnetic field at ϕ_{op} (B_a). At $B_a = 0.2$ T, the flux line density (d_{fl}) is calculated to be 1×10^{10}/cm^2. Assuming that each incident ion creates one columnar defect, and each columnar defect pins one flux line, the irradiation to a fluence of 1×10^{10} ions/cm^2 is considered to be sufficient. However, in reality, there is not much improvement in J_c at that fluence, and ϕ_{op} (0.2 T) is ~1×10^{11} ion/cm^2, ten times larger than d_{fl}. At $B_a = 2$ T, $d_{fl} = 1 \times 10^{11}$/cm^2, but ϕ_{op} (2 T) = 3 ~ 5×10^{11} ions /cm^2, which is three times larger than d_{fl}. This can be understood by follows using the schematic illustration shown in Fig. 14. While the defects introduced by heavy-ion irradiation have a random distribution, the flux lines try to form a triangular lattice as much as possible due to the repulsive force between the flux lines. So, it may be easier for the flux line to find an ideal position to form triangular lattice for higher pinning density and there for can obtain larger pinning force. However, when the fluence becomes higher (for example, 1×10^{12} ion/cm^2), the portion of damage area Y123 becomes large, resulting in the decrease of the superconducting volume and thus large decrease of J_c is observed.

The reason why Au-ion irradiation did not give a large improvement in J_c at $B_a = 2$ T may be understood by considering the decrease of the superconducting volume due to the irradiation defects. For example, for Au (Ag: 0 mm), Au (Ag: 5 mm), and

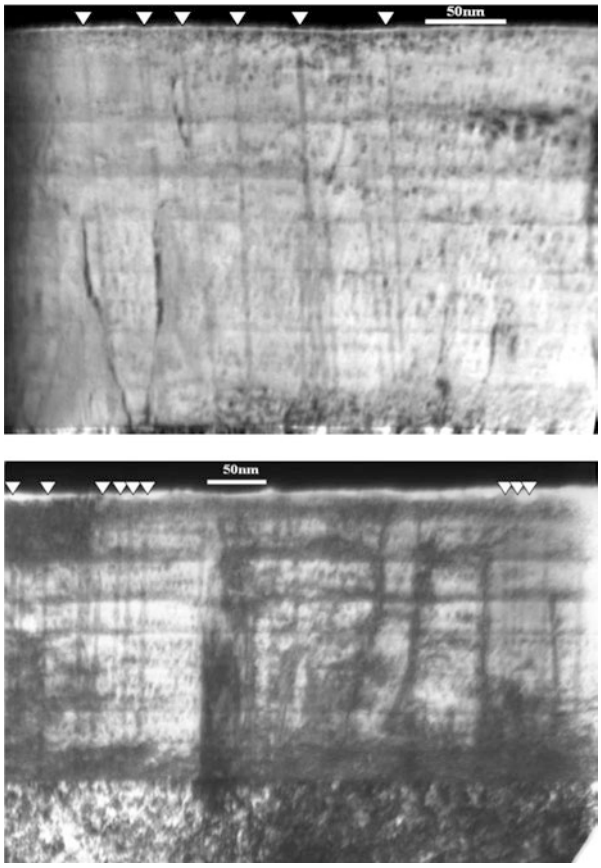

Fig. 12 TEM images of columnar defects in heavy-ion irradiated Y123 tapes. The locations of columnar defects are shown by white arrows. (**a**) 450 MeV $^{129}Xe^{23+}$ irradiation, fluence 1×10^{11} [ions/cm^2] (**b**) 500 MeV $^{197}Au^{31+}$ irradiation, fluence 1×10^{11} [ions/cm^2], Ag layer removed

Xe (Ag: 5 mm), the volume % of defects at irradiation fluence 5×10^{11} ions/ cm^2, assuming no the overlap of defects, is ~ 66%, ~ 47%, and ~ 25%, respectively, suggesting that the superconducting current path is significantly impeded.

In addition, large disturbance of Y123 crystal lattice is observed in Au-ion irradiated sample. Figure 15 shows the irradiation fluence dependence of normalized *c*-axis length, c/c_0, in which c_0 is the *c*-axis length before irradiation, and increase of FWHM (Full Width at Half Maximum) of (006) peak, ΔFWHM, of Y123 measured by X-ray diffraction measurement (XRD). We can see a remarkable extension of *c*-axis length as well as the increase of FWHM by Au-ion irradiation.

Figure 16 compares the Raman spectroscopy data for before and after irradiation with various species to the fluence of 1×10^{12} ions/ cm^2. We can see that the peaks around 335 and 500 cm^{-1} shifted to lower value by irradiation. It is known that these peaks are sensitive to oxygen defects, and result indicates the formation of oxygen

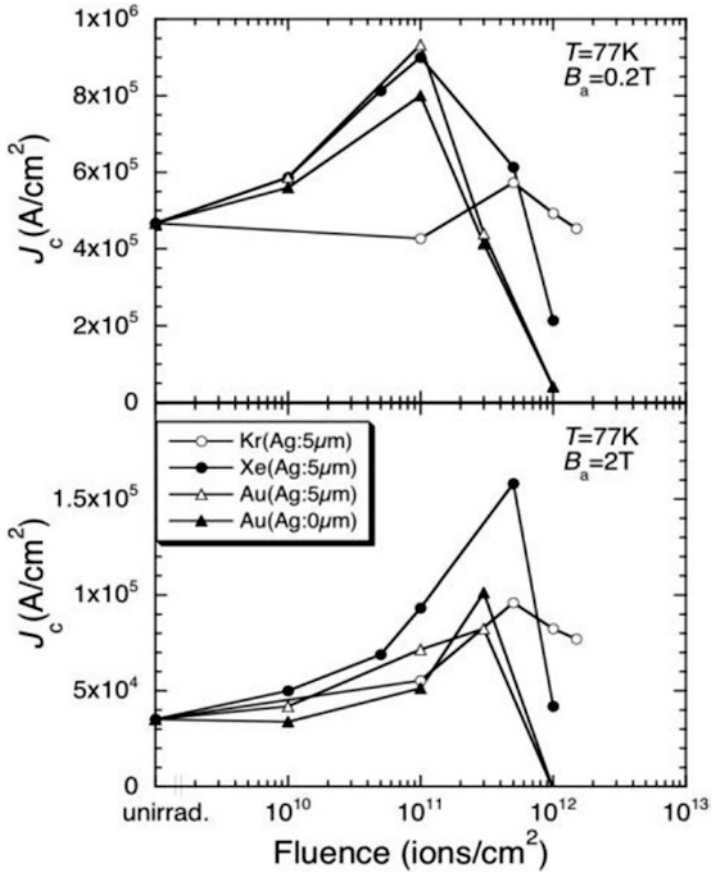

Fig. 13 Fluence dependence of J_c at 77 K for 400 MeV Kr-, 450 MeV Xe-, and 500 MeV Au-ion irradiations

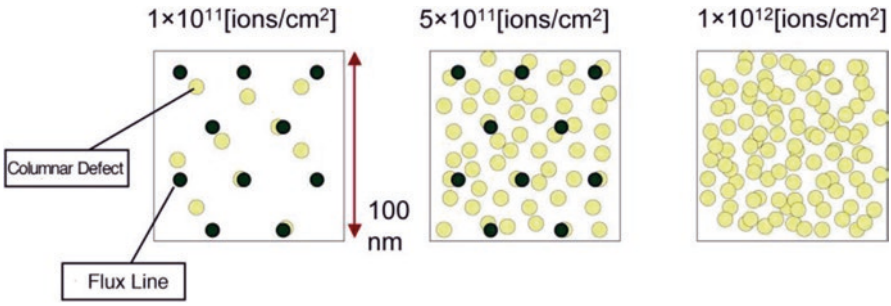

Fig. 14 Schematic illustration of the distribution of columnar defects and flux lines for B_a=2 T

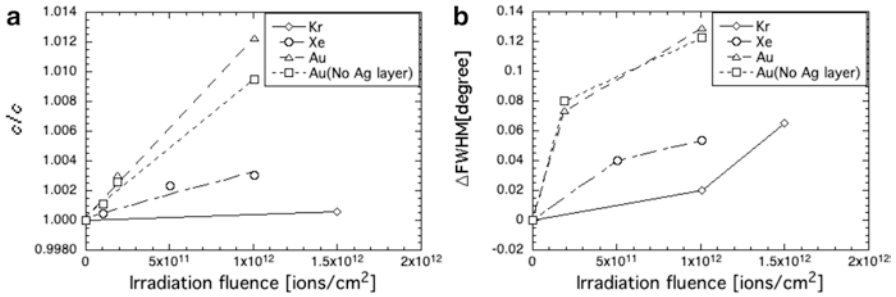

Fig. 15 Irradiation fluence dependence of c/c_0 (**a**) and ΔFWHM of (006) peak in XRD data (**b**)

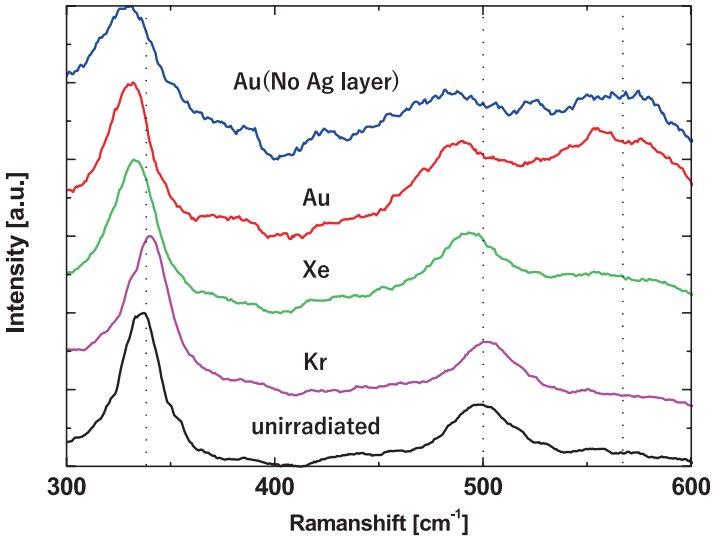

Fig. 16 Raman spectroscopy data for Y123 before and after irradiation. All the irradiation was performed at the same fluence 1×10^{12} ions/cm^2

vacancies by irradiation [26]. In addition, in Au-ion irradiated samples we observed an appearance of broad peak around 570 cm^{-1}. According the refs. [27, 28], this peak suggests the presence of cation disorder in Y123 layer.

We also measured T_c before and after irradiation. Figure 18 shows the fluence dependence of T_c for three different irradiation conditions. T_c are found to be almost constant at low fluences below 1.0×10^{11} ions/cm^2, while it decreases rapidly at a certain fluence, namely critical fluence, ϕ_{cr}, depending on the irradiated species. We can see that the smaller ϕ_{cr} for larger S_e, such as Au-ion irradiation.

From these results, we consider that not only the reduction of superconducting volume but also the reduction of superconducting condensation energy due to the introduction of the disorder inside the Y123 crystal lattice causes the reduction of J_c, in particular for Au-ion irradiation.

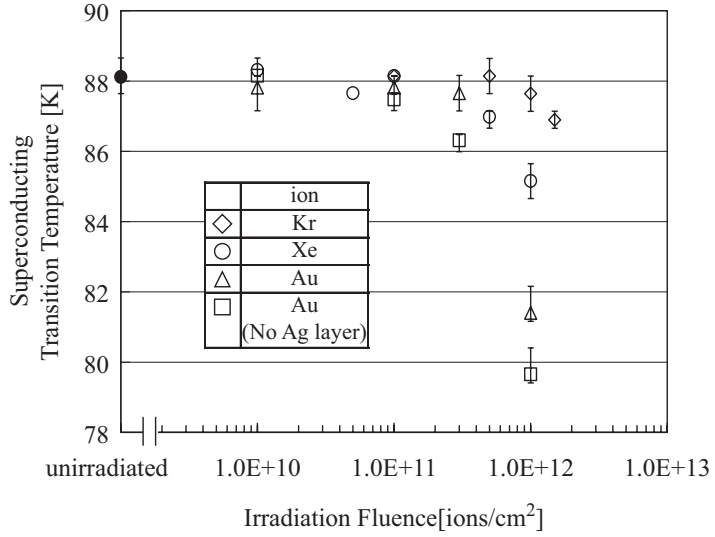

Fig. 17 Effect of heavy-ion irradiation on T_c in Y123 coated conductor

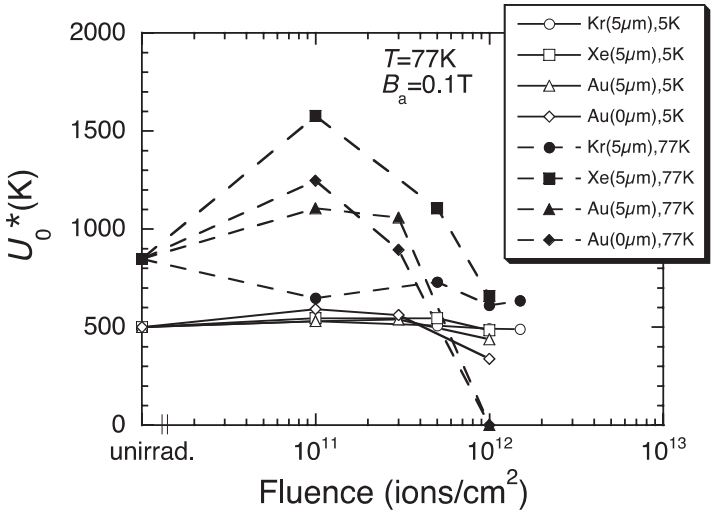

Fig. 18 Fluence dependence of U_0* at 77 K and 0.1 T for 400 MeV Kr-, 450 MeV Xe-, and 500 MeV Au-ion irradiations

Regarding Kr ion irradiation, there was almost no improvement in J_c at B_a = 0.2 T, whereas at B_a = 2 T, improvement in J_c was observed at a high fluence ~ 5 × 10^{11} ions/cm^2. In case of Kr ion irradiation, estimated size of columnar defect is about 4 nm, which is much smaller than the superconducting coherence length and the pinning force provided by the columnar defect is thought be the same order as

existing defects, such as spiral dislocations. In such situation, introduction of pinning center by irradiation is thought to be not effective for improving J_c in a low magnetic field because d_{fl} is much smaller than the total number of pinning centers. On the other hand, in a high magnetic field where d_{fl} exceeds the density of existing defects, the magnetic flux lines that were not pinned before irradiation will be pinned by the introduction of defects, leading to the improvement of J_c.

In order to verify this idea, magnetic flux creep measurement was performed and the change in apparent pin potential U_0^* due to heavy-ion irradiation was investigated. Flux creep measurement was performed as follows. At first, we applied a sufficiently high magnetic field (5 T) to give full penetration of flux line in the sample. Then we reduced the magnetic field to 0.1 T and then measured the time dependence of magnetization. U_0^* were obtained by using Anderson-Kim model [29, 30] from the magnetic relaxation results.

Figure 18 shows the fluence dependence of U_0^* at 5 K and 77 K of Kr, Xe, and Au-ion irradiated samples. At 5 K, there is no significant change in U_0^* due to irradiation, suggesting the pinning strength is almost the same as that of the existing defect.

On the other hand, at 77 K, U_0^* tends to increase at 10^{11} ions/cm^2 and decrease at larger fluences, except for Kr ion irradiation. Regarding Kr ion irradiation, there was almost no change in U_0^* due to irradiation. These results suggest that the columnar defect introduced by Au and Xe-ion irradiation has larger pinning potential in this temperature range, while the pinning potential of columnar defect introduced by Kr ion irradiation seems be comparable to existing defects.

4.2 *Effect of Post-Annealing in Heavy-Ion Irradiated RE123 Coated Conductors*

As discussed in the previous section, we consider that the reason for reduction of J_c in Au-ion irradiation is due to the reduction of superconducting condensation energy caused by the introduction of the disorder inside the Y123 crystal lattice.

In the present study, we performed post-annealing to anneal out introduced cation disorder and oxygen defects and to see if it is efficient for restoring superconducting properties. For this post-annealing process, selection of annealing temperature is very important. If the annealing temperature is too high, large deficiency of oxygen occurs in Y123 and the superconductivity will be lost. So, we chose two moderate temperature, 473 K and 673 K for the treatment. The annealing was performed in the flowing oxygen atmosphere for 2 h and then quenched.

Figure 19 shows the J_c values measured at B_a = 2.0 T before irradiation, after irradiation, and after annealing. We observed an increase of J_c after annealing at 673 K, while it was reduced at 473 K for 3.0×10^{11} ions/cm^2. On the other hand, in case of 1.0×10^{12} ions/cm^2, the decreased J_c by the irradiation did not recovered by the annealing. We also measured change in T_c after irradiation and annealing. As

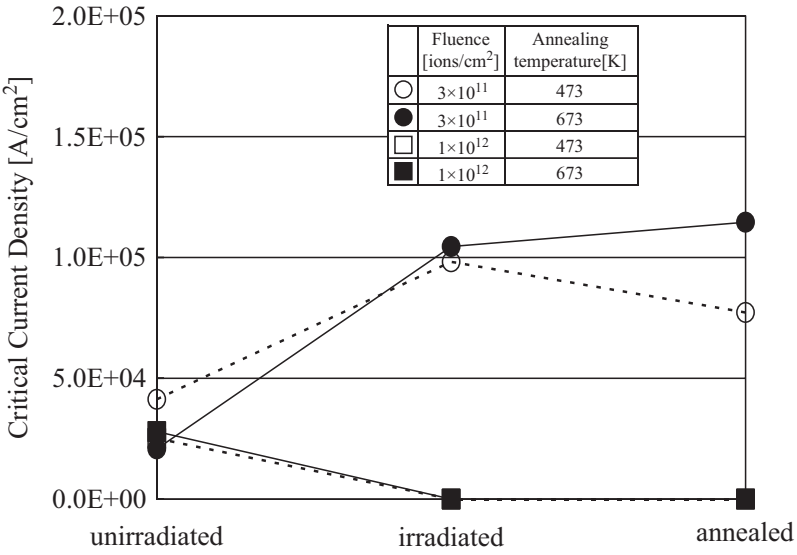

Fig. 19 Change in J_c at B_a = 2.0 T after Au-ion irradiation and post-annealing for Y123 (removed silver layer)

shown in Fig. 18, T_c was decreased by about 8 K after Au-ion irradiation (no Ag layer) with 1.0×10^{12} ions/cm^2. After annealing, we observed slight recovery of T_c, $\Delta T_c \sim 0.5$ K for 473 K and ~1 K for 673 K.

These results suggest that the post-annealing was a good way to recover T_c without decreasing J_c. However, optimization of annealing condition is required.

5 Summary

In this chapter, irradiation studies on La214 single crystals and Y123 coated conductor are reviewed. All of the results shown here lead to the conclusion that both neutron and heavy-ion irradiation are powerful tools for improving the pinning properties. Besides that, irradiation is also very effective in studying the pinning mechanism. In La214, there is big difference in J_c-B characteristics between neutron-irradiated sample and heavy-ion irradiated sample. The former causes so-called "fish-tail" type 2nd peak, while latter causes "matching effect" type 2nd peak in J_c-B curve.

In Y123 coated conductors, we examined the effect columnar defect size for the improvement of J_c. We modified the defect size by changing S_e. S_e is changed either by changing the ion species to be irradiated or by changing the thickness of Ag layer on top of Y123 layer. The enhancement of J_c was observed especially at the high magnetic field in 77 K, but the degree of the enhancement was different for the

irradiation condition. The largest enhancement of J_c at 77 K has been observed in case of the Xe-ion irradiation, whereas TRIM code calculation gives largest S_e value for Au-ion irradiation without Ag layer. XRD and Raman microscopy data suggested the introduction of the disorder inside the Y123 crystal lattice in Au-ion irradiated sample, which likely causes the depression of superconducting properties. This result suggests that we must carefully choose ion species that can create columnar defects without damaging crystallinity of Y123 layer. However, we show that post-annealing may be effective to recover the damage inside Y123 for further J_c improvement.

Acknowledgments The author would like to thank Dr. T. Kimura for La214 single crystals, Dr. A. Ibi for Y123 coated conductors, and Dr. M. Konczykowski for heavy- ion irradiation in GANIL. The irradiation and post-annealing of Y123 had been studied in collaboration with K. Nakashima and T. Terai.

References

1. *For example,* Wei-Kan Chu, Jia Rui Liu, Zu Hua Zhang, Nuclear instruments and methods in physics research section B: Beam interactions with materials and atoms 59–60, Part 2, 1447 (1991); L. Civale, Supercond. Sci. Technol. **10**, A11 (1997).
2. M.C. Frischherz, M.A. Kirk, J. Farmer, L.R. Greenwood, H.W. Weber, Physica C **232**, 309 (1994)
3. H.W. Weber, in *Proceedings of the 10th Anniversary HTS Workshop on Physics, Materials and Applications*, ed. by B. Batlogg, C.W. Chu et al., (World Scientific, Singapore, 1996) pp163 and references there in.
4. F.M. Sauerzopf, Phys. Rev. B **57**, 10959 (1998)
5. V. Hardy, D. Groult, M. Hervieu, J. Provost, B. Raveau, Nucl. Instrum. Methods B **54**, 472 (1991)
6. T. Kimura, K. Kishio, T. Kobayashi, Y. Nakayama, N. Motohira, K. Kitazawa, K. Yamafuji, Physica C **192**, 247 (1992)
7. T. Kobayashi, Y. Nakayama, T. Kimura, K. Kishio, K. Kitazawa, K. Yamafuji, Appl. Phys. Lett. **62**, 1830 (1993)
8. M. Daeumling, J.M. Seuntjens, D.C. Labalestier, Nature **346**, 332 (1990)
9. L. Krusin-Elbaum, L. Civale, V.M. Vinokur, F. Holtzberg, Phys. Rev. Lett. **69**, 2280 (1992)
10. T. Nishizaki, T. Naito, N. Kobayashi, Phys. Rev. B **58**, 11169 (1998) Physica C282-287, 2117(1997)
11. M. Xu, D.K. Finnemore, G.W. Crabtree, V.M. Vinokur, B. Dabrowski, D.G. Hinks, K. Zhang, Phys. Rev. B **48**, 10630 (1993)
12. N. Chikumoto, M. Konczykowski, N. Motohira, A.P. Malozemoff, Phys. Rev. Lett. **69**, 1260 (1992)
13. T. Tamegai, Y. Iye, I. Oguro, K. Kishio, Physica C **213**, 33 (1993)
14. G. Yang, P. Shang, S.D. Sutton, I.P. Jones, J.S. Abell, C.E. Gough, Phys. Rev. B **48**, 4054 (1993)
15. E. Zeldov, D. Majer, M. Konczykowski, A.I. Larkin, V.M. Vinokur, V.B. Geshkenbein, N. Chikumoto, H. Shtrikman, Europhys. Lett. **30**, 367 (1995)
16. V. Hardy, A. Wahl, A. Ruyter, M. Maignan, C. Martin, L. Coudrier, J. Provost, C. Simon, Physica C **232**, 347 (1994)
17. J.D. Jorgensen, P. Lightfoot, S. Pei, B. Dabrowski, D.R. Richards, D.G. Hinks, *Advances in Superconductivity III* (Springer-Verlag, Tokyo, 1990), p. 337

18. For review, T. Matsushita, in *Composite Superconductors* (Marcel Dekker Inc., New York, 1994), p. 21.
19. T. Matsushita, H. Kuepfer, J. Appl. Phys. **63**, 5048 (1988)
20. H. Tobita, K. Notoh, K. Higashikawa, M. Inoue, T. Kiss, T. Kato, T. Hirayama, M. Yoshizumi, T. Izumi, Y. Shiohara, Supercond. Sci. Technol. **25**, 062002 (2012)
21. J.L. Macmanus-Driscoll, S.R. Foltyn, Q.X. Jia, H. Wang, A. Serquis, L. Civale, B. Maiorov, M.E. Hawley, M.P. Maley, D.E. Peterson, Nat. Mater. **3**, 439 (2004)
22. S. Kang, A. Goyal, J. Li, A.A. Gapud, P.M. Martin, L. Heatherly, J.R. Thompson, D.K. Christen, F.A. List, M. Paranthaman, D.F. Lee, Science **311**, 1911 (2006)
23. Y. Zhu, Z.X. Cai, R.C. Budhani, M. Suenaga, D.O. Welch, Phys. Rev. B **48**, 6436 (1993)
24. T.E. Mitchell et al., Appl. Phys. Lett. **55**, 283 (1989)
25. E.M. Gyorgy, R.B. van Dover, K.A. Jackson, L.F. Schneemeyer, J.V. Waszczak, Appl. Phys. Lett. **55**, 283 (1989)
26. R.M. Macfarlane, H.J. Rosen, E.M. Engler, R.D. Jacowitz, V.Y. Lee, Phys. Rev. B **38**, 284 (1988)
27. G. Gibson, J.L. MacManus-Driscoll, L.F. Cohen, IEEE Trans. Appl. Supercond. **7**, 2130 (1997)
28. G. Gibson, L.F. Cohen, R.G. Humphreys, J.L. MacManus-Driscoll, Physica C **333**, 139 (2000)
29. P.W. Anderson, Y.B. Kim, Rev. Mod. Phys. **36**, 39 (1964)
30. R.A. Doyle, W.S. Seow, J.D. Johnson, A.M. Campbell, P. Berghuis, R.E. Somekh, J.E. Evetts, G. Wirth, J. Wiesner, Phys. Rev. B **51**, 12763 (1995)